J Wood Sci (2008) 54:267–277
DOI 10.1007/s10086-007-0938-0

ORIGINAL ARTICLE

Wook Kang · Woo Yang Chung · Chang-Deuk Eom
Hwanmyeong Yeo

Some considerations in heterogeneous nonisothermal transport models for wood: a numerical study

Received: September 5, 2007 / Accepted: November 26, 2007 / Published online: May 7, 2008

Abstract This study compares a number of coupled heat and mass transfer models and presents numerical comparisons of phenomenological coefficients between the four models (Stanish, Perre, Pang, and Avramidis) that are most frequently used in the literature to describe wood-drying processes. The USDA sorption isotherm, the Hailwood-Horrobin model, was adopted to calculate the relations between moisture content in wood and water vapor pressure at any temperature. Due to different assumptions about the driving forces of heat and mass transfer, coefficients in each model represent different values for moisture content and temperature and are closely related to each other. In the case of isothermal mass transfer, the moisture diffusion coefficient in the transverse directions from the Stanish and Pang models increased with decreasing moisture content. This contradicts the Avramidis and Perre models and numerous experimental results. Thermal diffusion effects on the drying process may not be predominant because the nonisothermal state is relatively short. Therefore, the Perre model, which does not consider the thermal diffusion effect, has been used successfully in the drying simulation. However, it may be erroneous in certain cases when the nonisothermal state prevails over the system, such as building physics. The Pang model cannot explain the phenomena of thermal diffusion and moisture thermodiffusion. It might be reasonable to modify the thermal diffusion of the Avramidis model, which is lower than that of the Stanish model. The apparent heat diffusivity was higher than the true heat diffusivity.

Key words Nonisothermal transport model · Drying · Building physics · Phenomenological coefficients · Sorption isotherm

W. Kang · W.Y. Chung
Division of Forest Resources and Landscape Architecture, Chonnam National University, Gwangju 561-756, Republic of Korea

C.-D. Eom · H. Yeo (✉)
Department of Forest Sciences, Research Institute for Agriculture and Life Sciences, Seoul National University, San 56-1, Sillim-dong, Gwanak-gu, Seoul 151-921, Republic of Korea
Tel. +82-2-880-4781; Fax +82-2-873-2318
e-mail: hyeo@snu.ac.kr

Introduction

Heat and mass transfer modeling is important for improving our knowledge of many engineering problems, such as the moisture-buffering capacity of wood in building physics,[1] wood drying, and wood-based panel manufacturing during hot pressing. Most of the sophisticated models have been developed within the wood-drying research field. Their importance is increasing because of the demand for wood components as building materials is expected to increase in the future and given that well-designed drying process control is required at present.

Moisture in wood exists in three phases: water vapor, bound water, and free water above the fiber saturation point (FSP). There are two phases of water vapor in the cell cavities and bound water in the cell walls, below FSP in the hygroscopic range. The maximum bound water content is at the FSP and is limited by the number of sorption sites available. This may differ among species because their chemical compositions vary, but it is usually assumed that FSP is 30% water, based on the wood's dry weight at room temperature.

It is well documented that the driving potential for the movement of free water and water vapor is the gradient of capillary pressure and vapor pressure, respectively. Furthermore, the flux of water vapor can be divided into the convection component of the gas mixture flux and the diffusion component of water vapor under the effect of a gradient in vapor concentration. However, the driving potential for the bound water differs according to researchers, and can be expressed in terms of a number of different system variables. Siau[2] stated that under isothermal conditions it does not matter which potential is used in the diffusion equation as long as the appropriate diffusion coefficient is used. The most commonly used potentials are based on the chemical potential and the gradient of bound water concentration.

Under nonisothermal conditions, thermally induced mass transfer (thermal diffusion or Soret effect) should be taken into account in models. This is because there might

be a significant temperature difference between the outer and inner surfaces of a building envelope, although this may be neglected in wood drying because the temperature change duration is relatively small.

In the literature, we can find three distinct formulations of nonisothermal transport models that are widely accepted in wood drying and other research fields. First, Avramidis et al.[3] developed Luikov-type equations mainly for modeling wood drying at low temperatures, and are based on a series of studies by Stamm,[4] Choong,[5] and Siau.[2,6] Avramidis assumed that mass transfer is driven by moisture and temperature gradients. He used the combined bound water diffusion coefficient that involves both bound water and water vapor movement. However, the model can be applied only below the hygroscopic range and at low temperature below the boiling point of water because he did not consider capillary movement above the hygroscopic range and water vapor convection after change of water state to vapor. Second, Perre's model[7] is based on Whitaker's multiphase transfer model[8] with an additional potential of bound water. Perre et al.[7] focused on heat and mass transfer modeling above the boiling point of water, in which mass transfer by gas convection is dominant. The bound water diffusion coefficient is based on Stamm's result,[4] which is similar to the Avramidis model. Third, Stanish[9] assumed that bound water diffusion is driven by the chemical potential, which makes his model different from Perre's model. It should be noted that both Stanish and Perre developed general models for nonhygroscopic as well as hygroscopic materials. Pang[10] focused mainly on high-temperature wood drying and he used the driving potential for bound water similar to the chemical potential of Stanish's model.

All the above models were compared for their ability to predict experimental results. Satisfactory agreements were obtained over given material and environmental conditions. However, not all the physical and transport coefficients were determined experimentally, and the validity would be uncontestable. The application of a model to various wood species might be questionable under a wide range of dynamic external conditions.

Kamke and Vanek[11] compared the capacities of 12 wood-drying models with the experimental drying results of moisture change rate and distribution that included the above three models (Avramidis, Perre, and Stanish). They stated that "none of the models violated any of the known wood-drying phenomena, but there was a high variability between models' results that was not in close agreement with the test runs. It might be due to uncertain coefficients for the models, different degrees of simplifications, and different ways of solving the heat and mass transfer equations." In addition, the equations for boundary conditions and external heat and mass convection coefficients are usually different among models, which might affect the numerical results. Yeo and Smith[12] developed the convective mass transfer coefficient conversion method, which proves that boundary-layer theory is useful for evaluating external moisture resistance during wood drying, using surface moisture data.

However, little work has been done on the numerical comparison of governing equations for heat and mass transfer models in wood because their assumptions and equation forms are different, and it is not easy to compare those differences explicitly between models. The objective of this study was to numerically compare four models in the hygroscopic range after modifying them to the same form of partial differential equations.

Formulation of the heat and mass transfer equation

Conservation of mass and energy

Stanish et al.[13] and Perre et al.[7] developed the three mass conservation equations for the multiphase mass transfer of bound water, water vapor, and air, as shown in Table 1 (the notation used in the equations and throughout the text is defined in Table 2). The fluxes of bound water differ between these two reports. In the hygroscopic range, Stanish et al.[13] assumed that the flux of bound water is proportional to the chemical potential and volume fraction of the cell wall, but Perre et al.[7] considered only the bound water diffusion. The vapor fluxes can be divided by gas convection and vapor diffusion, and they adopted similar assumptions.

However, the changes in air density and internal gaseous pressure can be neglected when modeling heat and mass transfer below the boiling point of water. This assumption enables the three conservation equations to be simplified to two conservation equations and the flux of water vapor can be redefined by assuming the air flux is negligible:[13]

$$J_v = -\frac{M_v}{RT\left(1-P_v/P_g\right)}\bar{\bar{D}}_{eff}\nabla P_v \tag{1}$$

Table 1. Comparison of fluxes defined by Stanish et al. and Perre et al.

Flux	Stanish[a]	Perre[b]
J_b	$-D_{bS}(1-\phi)\frac{1}{M_v}\left(\frac{RT}{P_v}\nabla P_v - S_v\nabla T\right)$	$-\rho_{ow}D_{bP}\nabla m$
J_v	$-\rho_v\frac{K_g}{\mu_g}\nabla P_g - \frac{M_v}{RT(1-P_v/P_g)}\bar{\bar{D}}_{eff}P_g\nabla\left(\frac{P_v}{P_g}\right)$	$-\rho_v\frac{K_g}{\mu_g}\nabla P_g - \rho_g\bar{\bar{D}}_{eff}\nabla\left(\frac{\rho_v}{\rho_g}\right)$
J_a	$-\rho_a\frac{K_g}{\mu_g}\nabla P_g - \frac{M_a}{RT(1-P_a/P_g)}\bar{\bar{D}}_{eff}P_g\nabla\left(\frac{P_a}{P_g}\right)$	$-\rho_a\frac{K_g}{\mu_g}\nabla P_g - \rho_g\bar{\bar{D}}_{eff}\nabla\left(\frac{\rho_a}{\rho_g}\right)$

[a] Stanish et al.[13]
[b] Perre et al.[7]

Table 2. Definitions of notation

Notation	Definition	Unit or known value
C_p	Specific heat of wood	J/kg K
C_{pa}	Specific heat of air	J/kg K
C_{pv}	Specific heat of water vapor	J/kg K
D_v	Bulk binary diffusivity of water vapor in air	m^2/s
D_b	Diffusion coefficient of wood	m^2/s
D_{bS}	Stanish diffusion coefficient	m^2/s
D_{bP}	Perre diffusion coefficient	m^2/s
D_{bR}	Pang diffusion coefficient	m^2/s
D_{bL}	Diffusion coefficient of bound water in longitudinal direction	m^2/s
D_{bT}	Diffusion coefficient of bound water in transverse direction	m^2/s
E_a	Energy to dissociate a mole of sorbed water from sorption sites	J/mol
E_b	Activation energy ($38500 - 29000\,m$)	J/mol
E_v	Molar latent heat of evaporation	J/mol
E_w	Activation energy of liquid water	J/mol
E_s	Molar differential heat of sorption	J/mol
G_{ow}	Specific gravity of oven-dried wood	Dimensionless
h_b	Enthalpy of bound water	J/kg
h_v	Enthalpy of water vapor	J/kg
Δh_v	Latent heat of evaporation	J/kg
Δh_s	Differential heat of sorption	J/kg
J_b	Flux of bound water	kg/m^2 s
J_v	Flux of water vapor	kg/m^2 s
J_a	Flux of air	kg/m^2 s
K_v	Permeability of water vapor	m^2
m	Fractional moisture content	Dimensionless
M_v	Molecular weight of water vapor	kg/mol
P_v	Partial vapor pressure	Pa
P_{vs}	Saturated vapor pressure	Pa
R	Universal gas constant	8.314 J/mol K
S_v	Entropy of water vapor	J/mol K
T	Temperature	K
α	Tortuosity, attenuation factor for water vapor diffusivity	Dimensionless
φ	Relative humidity	Dimensionless
λ_{eff}	Effective thermal conductivity	W/m K
ϕ	Porosity or void fraction	Dimensionless
ρ	Wood density	kg/m^3
ρ_{ow}	Wood density of oven-dried wood	kg/m^3
ρ_v	Density of water vapor	kg/m^3
ρ_w	Liquid water density	kg/m^3
ρ_a	Air density	kg/m^3
μ_{vs}	Chemical potential of saturated vapor	J/mol
μ_b	Chemical potential of bound water	J/mol
μ_w	Chemical potential of liquid water	J/mol
μ_g	Dynamic viscosity of air	N s/m^2
μ_v	Dynamic viscosity of water vapor	N s/m^2

Furthermore, the gradient of water vapor can be reduced to one of water vapor pressure by using the ideal gas law:[7]

$$J_v = -\frac{M_v}{RT}\bar{\bar{D}}_{eff}\nabla P_v \tag{2}$$

The effective vapor diffusivity and bulk binary diffusivity of water vapor in air is given by:

$$\bar{\bar{D}}_{eff} = \alpha\phi D_v \tag{3}$$

$$D_v = 2.20\times10^{-5}\left(\frac{T}{273.15}\right)^{1.75}\left(\frac{101325}{P_g}\right) \tag{4}$$

Bories[14] stated that the attenuation factor for effective vapor diffusivity through porous media depends on the material's texture (tortuosity, porosity distribution, anisotropy), moisture content, and experimental conditions. Akanni and Evans[15] reviewed the tortuosity factor employed frequently for porous solids, and represented it as a function of porosity. However, the coefficient remains unknown and differs among researchers.

Stanish[9] adapted values of α of 0.05 and 0.01 for southern pine and Douglas fir, respectively. This study assumed α to be 0.03 for the Stanish model. In the Perre model, $\alpha\phi$ was adapted to be 0.001 to include the effect of porosity, and α is much lower than that used by Stanish.[9]

Because this study focuses on comparisons of the models only in the hygroscopic range and below the boiling point of water, the effect of gas convection can be neglected. Therefore, the change rate of water is equal to the total flux of bound water and water vapor. The mass transfer equation can be represented by:

$$\rho_{ow}\frac{\partial m}{\partial t} = -\nabla\cdot(\mathbf{J}_b + \mathbf{J}_v) \tag{5}$$

The heat-transfer equation can be represented using the energy conservation law.

$$\rho C_p \frac{\partial T}{\partial t} = \nabla \cdot (\lambda_{eff} \nabla T) - \nabla \cdot (\mathrm{J}_b h_b + \mathrm{J}_v h_v) \quad (6)$$

where the density, specific heat, and thermal conductivity of wood with changing moisture are calculated using equations proposed by Forest Products Laboratory.[16]

$$\rho = \frac{\rho_{ow}(1+m)}{(1+mG_{ow})} \quad (7)$$

$$C_p = \frac{103.1 + 3.867T + 4190m}{1+m} + m(-6191 + 23.6T - 1330m) \quad (8)$$

$$\lambda_{eff} = \frac{G_{ow}}{1+mG_{ow}}(0.1941 + 0.4064m) + 0.01864 \quad (9)$$

Modification of models

Water vapor pressure is a function of moisture content and temperature, and is the product of relative humidity and saturated vapor pressure.

$$\nabla P_v = \frac{\partial P_v}{\partial m}\nabla m + \frac{\partial P_v}{\partial T}\nabla T \quad (10)$$

$$P_v = \varphi(m,T) P_{vs}(T) \quad (11)$$

The saturated vapor pressure is a function of temperature only, but the relative humidity in a material is a function of both moisture content and temperature, which can be obtained only from the measurement of the sorption isotherm. Furthermore, vapor pressure with respect to temperature is a function of relative humidity and saturation vapor pressure.

$$\nabla P_v = P_{vs}\frac{\partial \varphi}{\partial m}\nabla m + P_{vs}\frac{\partial \varphi}{\partial T}\nabla T + \varphi\frac{\partial P_{vs}}{\partial T}\nabla T \quad (12)$$

$$\nabla P_v = u\nabla m + v\nabla T \quad (13)$$

By substituting Eq. 13 for the gradient of partial vapor pressure into the expressions for the fluxes, simultaneous heat and mass transfer equations with two state variables, moisture content and temperature, can be represented.

$$\rho_{ow}\frac{\partial m}{\partial t} = \nabla \cdot (a_{11}\nabla m) + \nabla \cdot (a_{12}\nabla T) \quad (14)$$

$$\rho C_p \frac{\partial T}{\partial t} = \nabla \cdot (a_{21}\nabla m) + \nabla \cdot (a_{22}\nabla T) \quad (15)$$

To compare the transfer behaviors between models and materials, Eqs. 14 and 15 can be arranged to:

$$\frac{\partial m}{\partial t} = \nabla \cdot (K_{11}\nabla m) + \nabla \cdot (K_{12}\nabla T) \quad (16)$$

$$\frac{\partial T}{\partial t} = \nabla \cdot (K_{21}\nabla m) + \nabla \cdot (K_{22}\nabla T) \quad (17)$$

It should be noted that the shrinkage or swelling of wood and the change in density and specific heat with time were neglected in Eqs. 14 and 15. Equation 17 is not appropriate for solving because the density and specific heat are functions of moisture content.

By some mathematical manipulations, the heat and mass transfer coefficients of the Stanish and Perre models can be rearranged as shown in Table 3. The four transfer coefficients given by Pang are available directly from his report, and those of Avramidis et al.[3] are simply derived after modifying the mass transfer rate of the energy conservation equation.

Results and discussion

Moisture diffusion

For the transfer coefficients of the Stanish, Perre, and Pang models, the sorption isotherm at a given temperature should be known previously. The Hailwood-Horrobin sorption model by Simpson[17] was used to calculate the thermodynamic coefficients (u, v, η, ζ) as shown in Fig. 1. It should be noted that the sorption data are approximate means of the adsorption and desorption data, which are based on spruce grown in North America. Therefore, the model may have some deviations for other species, especially in hardwoods.

Changes in η and ς with temperature are very small, and η is always negative over the whole hygroscopic range because

$$\frac{RT}{P_v}\frac{\partial P_v}{\partial T} < S_v \quad (18)$$

Bound water diffusion within cell wall

After sealing off the lumens with molten bismuth, Stamm[18] first measured D_{BL}, bound water diffusion coefficients of the cell wall in the fiber direction. The adsorption tests were conducted at 26.7°C. Using Stamm's data, Siau[2] converted to D_{bT} by assuming $D_{bT} = D_{bL}/2.5$, and obtained the Arrhenius-type equation with the least-squares method.

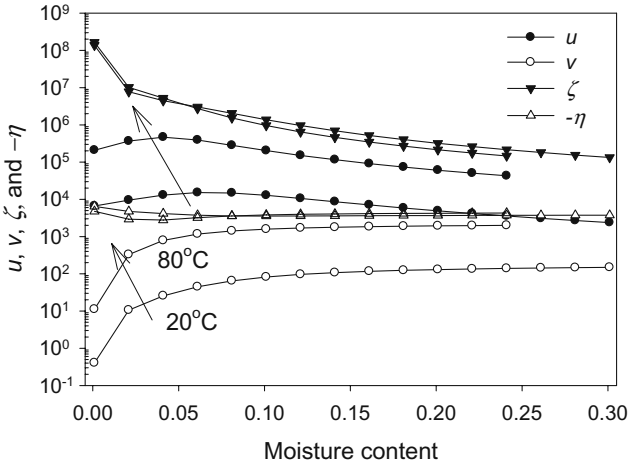

Fig. 1. Thermodynamic coefficients based on Hailwood-Horrobin model by Simpson[17]

Table 3. Heat and mass transfer coefficients below fiber saturation point for each model

Model	K_{11} (m^2/s)	K_{12} (m^2/s K)	K_{21} (m^2 K/s)	K_{22} (m^2/s)
Stanish[a]	$\frac{D_{\delta S}(1-\phi)}{\rho_{ow}}\varsigma+\frac{u}{\rho_{ow}}\frac{D_v}{(1-P_v/p_g)}$	$\frac{D_{\delta S}(1-\phi)}{\rho_{ow}}\eta+\frac{v}{\rho_{ow}}\frac{D_v}{(1-P_v/P_g)}$	$\frac{1}{\rho C_p}\left(h_b D_{\delta S}(1-\phi)\varsigma+\frac{h_v D_v u}{(1-P_v/P_g)}\right)$	$\frac{1}{\rho C_p}\left(\lambda_{eff}+h_b D_{\delta S}(1-\phi)\eta+\frac{h_v D_v v}{(1-P_v/P_g)}\right)$
Perre[b]	$D_{bP}+\frac{u}{\rho_{ow}}D_v$	$\frac{v}{\rho_{ow}}D_v$	$\frac{1}{\rho C_p}(h_b\rho_{ow}D_{bP}+h_v D_v u)$	$\frac{1}{\rho C_p}(\lambda_{eff}+h_v D_v v)$
Pang[c]	$\frac{D_{bR}(1-\phi)}{\rho_{ow}}\varsigma+\frac{u}{\rho_{ow}}\frac{K_v\rho_v}{\mu_v}$	$\frac{D_{bR}(1-\phi)}{\rho_{ow}}\eta+\frac{v}{\rho_{ow}}\frac{K_v\rho_v}{\mu_v}$	$\frac{1}{\rho C_p}\frac{u}{\rho C_p}\frac{K_v\rho_v}{\mu_v}\Delta h_v$	$\frac{1}{\rho C_p}\left(\lambda_{eff}+\Delta h_v v\frac{K_v\rho_v}{\mu_v}\right)$
Avramidis[d]	$\frac{7\times10^{-6}\exp(-E_b/RT)}{(1-\phi)(1-\sqrt{\phi})}$	δ_T	$\frac{E_b}{0.018C_p}K_{11}$	$\frac{1}{\rho C_p}\left(\lambda_{eff}+\frac{E_b\rho C_p}{0.018C_p}\delta_T\right)$

[a] Stanish et al.[13]
[b] Perre et al.[7]
[c] Pang[10]
[d] Avramidis et al.[3]

$$\delta_T=\left(\frac{d\mu_{vs}}{dT}+\frac{E_b+E_0+E_L}{T}+R\ln(\varphi)\right)\left(\frac{K_{11}\varphi}{RT}\right)\left(\frac{\partial m}{\partial\varphi}\right),\ E_b=38\,500-29\,000\,m,\ E_b=38500-29000m,\ \frac{d\mu_{vs}}{dT}=-63.35-75.31\ln\left(\frac{T}{273.15}\right)$$

$$D_v=\frac{M_v\bar{D}_{eff}}{RT},\ u(m,T)=\frac{\partial P_v}{\partial m}=P_{vs}\frac{\partial\varphi}{\partial m},\ v(m,T)=\frac{\partial P_v}{\partial T}=P_{vs}\frac{\partial\varphi}{\partial T}+\varphi\frac{\partial P_{vs}}{\partial T}$$

$$\eta=\frac{1}{M_v}\left(\frac{RT}{P_v}v(m,T)-S_v\right)=\frac{1}{M_v}\left(\frac{RT}{\varphi}\frac{\partial\varphi}{\partial T}+\frac{RT\varphi}{P_v}\frac{\partial P_{vs}}{\partial T}-S_v\right),\ \varsigma=\frac{RT}{M_v P_v}u(m,T)=\frac{RT}{M_v\varphi}\frac{\partial\varphi}{\partial m},$$

$$S_v=187+C_{pv}\ln\left(\frac{T}{298.15}\right)-R\cdot\ln\left(\frac{P_v}{101325}\right)$$

$$D_{bT}=7\times10^{-6}\exp\left(-\frac{E_b}{RT}\right) \tag{19}$$

$$D_{bT}=\exp\left(-11.8696+3488.1\frac{m}{T}-\frac{4631}{T}\right) \tag{20}$$

The above diffusion coefficients would give lower values when applied to wood drying because they are based on adsorption data under conditions of low air velocity.[6] In addition, the surface resistance was neglected and it was assumed that the surface comes to immediate moisture equilibrium with the surrounding atmosphere. Furthermore, the molten metal did not fill all the cavities completely. Nevertheless, this equation has been used widely in the field of wood research.

Perre and Turner[19] also used Stamm's data to calculate the diffusion coefficient of bound water but they did not adopt the activation energy, resulting in a slightly different form of equation.

$$D_{bT}=\exp\left(-12.8183933+10.8951601m-\frac{4300}{T}\right) \tag{21}$$

However, the coefficients given by Eqs. 19–21 are close to the experimental results found by Stamm[18] at 26.7°C, and change little at higher temperatures, as shown in Fig. 2. They increase with increasing moisture content and temperature.

The activation energy is one of the kinetic energies that is necessary for the bound water to move from one sorption site to another, which is lower than the energy needed to evaporate bound water. However, its physical meaning seems to be unambiguous because it can be measured only by diffusion coefficient experiments and their gradient by temperature.

$$E_b=-R\left[\frac{\partial(\ln D)}{\partial(1/I)}\right]_m=RT^2\left[\frac{\partial(\ln D)}{\partial T}\right]_m \tag{22}$$

Nelson[20,21] investigated the activation energy of bound water theoretically. He stated that it consists of the energy needed to dissociate a mole of sorbed water from sorption sites (E_a) and the activation energy of liquid water (E_w). E_a

Fig. 2. Bound water diffusion coefficient of cell wall in the transverse direction with moisture content and temperature

consists of E_v and RT/n. The former is the energy change from the sorbed state to the liquid state, and the latter is the energy change from the liquid state to the activated state.

$$E_b = E_v + \frac{RT}{n} + E_w = E_v + \frac{RT}{0.7} + 22175 \quad (23)$$

According to Nelson,[19,20] the transverse diffusion coefficient of bound water can be expressed as:

$$D_{bT} = \left(\frac{7.88\times10^{-6}}{2-0.9m/(0.685+0.9m)}\right)\left(\frac{0.685+0.9m}{2.653+0.9m}\right)\exp\left(\frac{-E_b}{RT}\right) \quad (24)$$

At 26.7°C, Fig. 2 shows that there is good agreement between Nelson's model and Stamm's experimental results, but there is a tendency to underestimate the diffusion coefficient of bound water at lower moisture content levels and to overestimate at higher ones. At higher temperatures, there is rather good agreement between the three models in the range of $m > 0.1$, but Eq. 24 represents a lower value than the other two models when $m < 0.1$.

Equation 24 is somewhat different from Eqs. 19–21 because E_v changes exponentially as a function of moisture content. The concept of Nelson's model is useful for estimating E_b by wood species because E_v may depend on the physicochemical properties of wood and a given specimen.

Combined bound water diffusion

The conductivity of bound water depends on bound water diffusion through the cell walls and water vapor diffusion into the cell cavities. As discussed by Choong,[5] the transverse moisture movement mechanism is dominated by cross-wall diffusion, which increases as moisture contents increase; whereas the longitudinal mechanism is dominated by vapor diffusion in the cell lumens, which decreases as moisture contents increase. This is supported by many experimental results, as shown in Fig. 3 and Table 4, and also by Danvind and Ekevad.[22]

The theoretical diffusion coefficient from the Avramidis model used in this study originates from Siau.[2] It can be predicted more precisely for softwood, such as Scotch pine than for hardwood, such as aspen and red oak.

For convenience, the specific gravity of wood is assumed to be 0.40 for the calculation of heat and mass transfer coefficients in this study. The combined or effective transverse diffusion coefficients of bound water (K_{11}) for each model are shown in Fig. 4. The parameters necessary for the models are adopted in the literature as:

$D_{bS}(kg\cdot s/m^3) = 3.0\times10^{-13}$ Stanish model

$D_{bP}(m^2/s) = \exp\left(-9.9+9.8m-\frac{4300}{T}\right)$ Perre model

$D_{bR}(kg\cdot s/m^3) = 8.0\times10^{-13}$ and $K_v(m^2) = 1.0\times10^{-15}$ Pang model

The transverse effective moisture diffusion coefficients in the Avramidis and Perre models are similar and increase with increasing moisture content, because it is assumed that Perre included the porosity effect on D_{bP}, and that the water vapor effect through the pit, D_v, is very small because $\alpha\phi = 0.001$. K_{11} in the Avramidis model is based on Siau,[2] which did not consider the effect of tortuosity and assumed that $\alpha = 1.0$.

However, the coefficients from Stanish's and Pang's models decrease with increasing moisture content because D_{bS} and D_{bR} are constant, but ζ, u, and D_v decrease with increasing moisture content, which disagrees with most of the previous experimental results. All the models considered in this study assume that all the phases are at the same temperature and that the partial vapor pressure is equal to its equilibrium pressure, whose condition is said to be in local thermodynamic equilibrium.

Stamm[4] proposed an electrical model to simulate moisture transfer in the hygroscopic range (Fig. 5), shown in

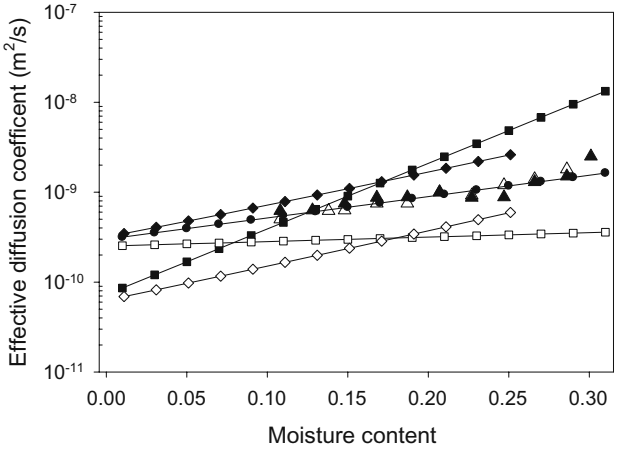

Fig. 3. Comparison of transverse effective diffusion coefficients by theory and experiments during desorption at 60°C. *Filled circles*, Scots pine;[26] *filled triangles*, Scots pine;[27] *open triangles*, Scots pine;[27] *filled squares*, aspen (transverse);[28] *open squares*, red oak (transverse);[29] *filled diamonds*, theoretical (SG 0.30);[2] *open diamonds*, theoretical (SG 0.65)[2]

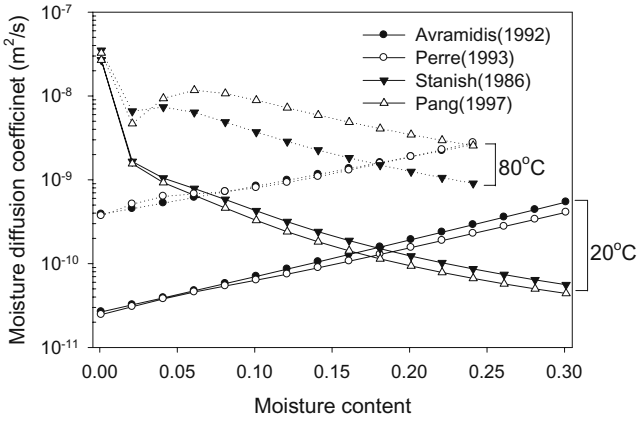

Fig. 4. Transverse effective moisture diffusion coefficients of wood with oven drying and specific gravity of 0.4 at 20°C and 80°C

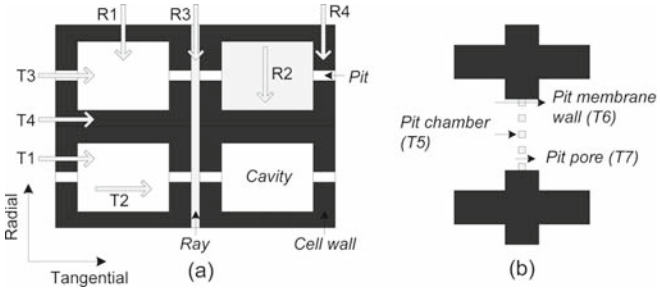

Fig. 5. a Primary paths for tangential and radial moisture transport through a cell wall and **b** secondary paths through a pit[5]

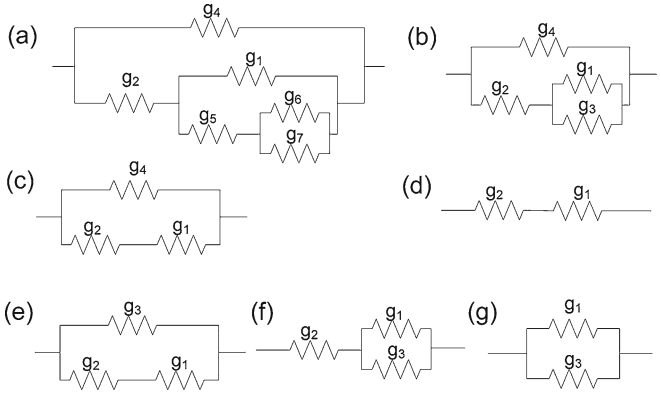

Fig. 6a–g. The electrical analog models for the paths of tangential moisture transport

Fig. 6a. Figure 6b shows a simplified model integrating secondary paths through a pit. Because the resistance of T3 and T4 is large, Siau[2] neglected their effects and adopted the model shown in Fig. 6d. As Siau stated, the effect of T3 may be important in woods with high permeability and high specific gravity, particularly at low moisture content and high temperature. The contribution of the pits in hardwood is expected to be less than in softwood because of the smaller pit openings in hardwoods.

However, Perre et al.[7] considered T3 in their model and used the model from Fig. 6e, although Fig. 6f may be more suitable for woods according to Stamm's theory. Stanish and Pang considered the movement of bound water and water vapor in the cavity by including the contribution of the pits as parallel paths. They adopted the model in Fig. 6g, and water vapor transfer through both the cavity and pit is more dominant than bound water. Therefore, their models are subject to some limitations for wood in the transverse direction and may be more suitable for moisture transfer through wood in the fiber direction, wood-based panels (e.g., medium-density fiberboard and particleboard), and homogeneous porous material. For the models of Stanish and Pang, the dependence of combined diffusion coefficient on moisture content does not change even if the bound water and water vapor transfer is transformed to series diffusion such as Fig. 6d.

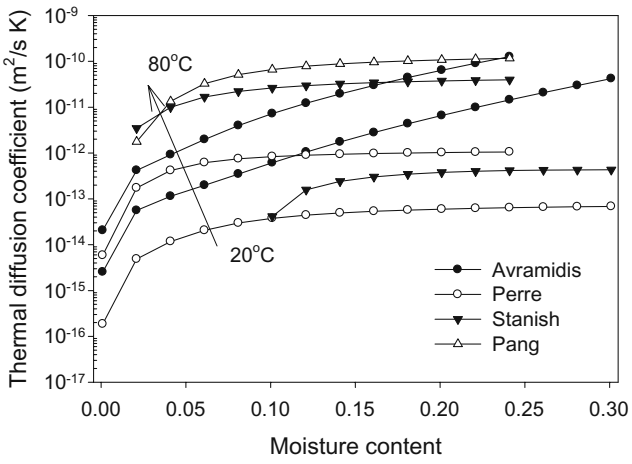

Fig. 7. Thermal diffusion coefficients of wood with oven-dried specific gravity of 0.4 at 20°C and 80°C

Thermal diffusion coefficient

Moisture is transported in the direction from higher temperature to lower temperature, although there is no moisture gradient within a material, and is known as thermal diffusion or the Soret effect. Thermal diffusion is more important in building physics than drying because wood in service is rarely maintained in an isothermal state, and the nonisothermal state is relatively short during drying.

It should be noted that the Avramidis model originates from Siau,[2] and Perre's model did not consider the thermal diffusion effect. Stanish et al.[13] compared their model to the experimental data from the literature.

The thermal diffusion coefficients (K_{12}) of the three models are shown in Fig. 7, except for Pang's model, whose value is several orders of magnitude lower than K_{11}. These coefficients are found to increase with increasing moisture content and are observed to be higher in higher temperature ranges. Pang's model has a negative value in the entire hygroscopic range because $-D_{bR}(1-\phi)\eta > vK_v\rho_v/\mu_v$, which contradicts the phenomenological observation that moisture flows in the direction of decreasing temperature. The Stanish model also has a negative value at low moisture content due to the large entropy value of water vapor.

In the steady state, the Soret effect can be calculated by using $dm/dT = -K_{12}/K_{11}$ (Fig. 8). In the nonisothermal state, the moisture transfer rate decreases with increasing $-dm/dT$ during drying, when the environmental temperature is higher than the material temperature.

The Avramidis model shows a higher value than Stanish's model at 20°C, but it is close to the Stanish model at 80°C because there is little change with temperature in the Avramidis model. These two models show that the value increases with moisture content; however, it decreases with moisture content in the Perre model, and gives a constant value near zero over the whole moisture range. Therefore, Perre's model cannot explain the Soret effect in steady state experiments.

Figure 9 shows the results of comparison of the Avramidis, Stanish, and other models, and the relevant equations from the literature are shown in detail in Table 5.

Stanish[9] compared his model to Models 2 and 7 in the unsteady state. As he stated, the accuracy of Model 7 must be questionable because it has a negative value over the whole moisture range. Peralta and Skaar[23] compared the steady-state uniaxial moisture profiles to those predicted by five different theoretical models. Models 9 and 5 provided the best results. Model 4 gave the next best prediction, followed by Model 6 (which is based on the Stanish model), and the last was Model 2. Siau and Avramidis[24] compared three models (2, 8, and 9); Model 9 provided the best fit to the experimental results, and Model 2 gave the poorest results.

There is little difference between Models 5 and 9 below moisture content of 0.2%, but they deviate greatly above that. Model 1 does not consider the material's hygroscopic properties, so with hygroscopic material $-dm/dT$ should be lower than that in Model 1. Avramidis and Hatzikiriakos[25] compared Models 4 and 9 with drying experiments and concluded that the thermodiffusion coefficient of Model 9 resulted in the best fit with the moisture and temperature data. Therefore, it may be concluded from the above research that Model 9 is the best one to use for the nonisothermal modeling.

Equation 23 and Model 5 show that the diffusion coefficient of bound water decreases, and the Soret effect increases as the differential heat of sorption increases.

Heat diffusion and moisture thermodiffusion

The same values of volume heat capacity (ρC_p) and heat transfer coefficient (λ_{eff}) were adapted to all the models. As shown in Table 3, however, the additional term of heat diffusion coefficient (K_{22}) made the thermal conductivity vary between models because the condensation or sorption heat occurs in the direction of increasing temperature as the moisture content increases or decreases. As shown in Fig. 10, Perre's and Pang's models at all temperatures, and Stanish's model at 20°C, show similar trends, with K_{22} decreasing at increasing moisture content, which was very close to the changes in $\lambda_{eff}/\rho C_p$. However, in Stanish's model it remains constant with moisture content at higher temperature (80°C), whereas in the Avramidis model there is a trend of

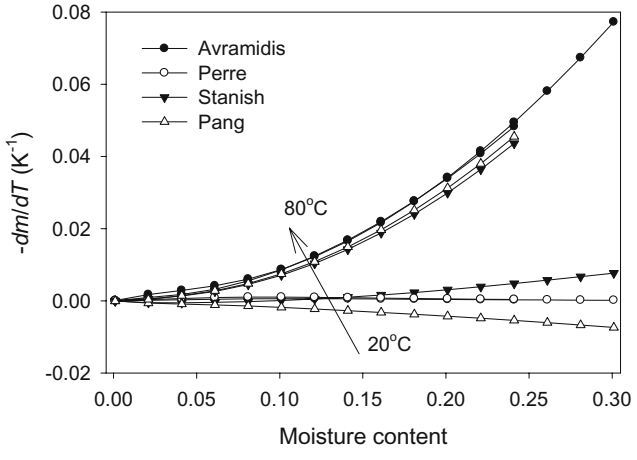

Fig. 8. Plot of $-dm/dT$ against moisture content with oven-dried specific gravity of 0.4 at 20°C and 80°C

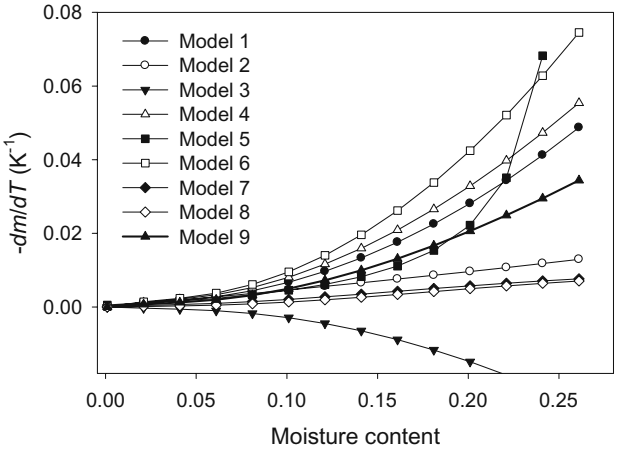

Fig. 9. Plot of $-dm/dT$ against moisture content with oven-dried specific gravity of 0.4 at 50°C

Table 4. Comparison of parameters in effective diffusion equation $D_b = D_0 exp(aX + b)$ from experimental results in the literature

D_0 (m²/s)	a	b	Experimental conditions			Literature cited
			Direction	Temperature (°C)	Species	
325×10^{-10}	–28.2	0	Longitudinal	30	Western fir	Choong[5]
171×10^{-10}	–13.3	0	Longitudinal	23.9	Yellow poplar	Rosen[30]
0.53×10^{-10}	0	0	Tangential	20	American beech	Skaar[31]
0.27×10^{-10}	6.5	0	Radial	20	American beech	Skaar[31]
0.044×10^{-10}	13.8	0	Tangential	26.7	Sitka spruce	Stamm[4]
0.27×10^{-10}	18.4	0	Tangential	40	Yellow poplar	Comstock[32]
5.55×10^{-4}	16.8	$-5280/T$	Transverse	43	Aspen	Simpson and Liu[28]
19.2×10^{-4}	1.15	$-5280/T$	Transverse	43	Red oak	Simpson[29]
16.0×10^{-4}	1.45	$-5280/T$	Transverse[a]	43	Red oak	Simpson[29]
6.34×10^{-14}	5.46	$2.54 \times 10^{-2} T$	Transverse	20/50/80	Scots pine	Hukka[26]
4.06×10^{-14}	5.32	$2.66 \times 10^{-2} T$	Transverse	20/50/80	Norway spruce	Hukka[26]

[a] Adsorption

Table 5. Comparison of the ratio of moisture content gradient to temperature gradient (*dm/dT*) from the literature

Model	Equation	Literature cited
1	$-\frac{v}{u}$	Bramhall[33]
2	$-\frac{E_b}{\frac{RT^2}{m}-\left(\frac{\partial E_b}{\partial m}\right)_T}$	Skaar and Siau[34]
3	$-\frac{\varphi\left(T\frac{d\mu_w}{dT}+E_s+RT\ln(\varphi)\right)}{C}$	Siau[35]
4	$-\frac{\varphi\left(T\frac{d\mu_w}{dT}+E_b+E_v+E_s+RT\ln(\varphi)\right)}{C}$	Siau and Zin[36]
5	$\frac{E_v+E_s-C_{pv}T}{(-1.038-0.049T)(-RT\ln\varphi)T}$	Nelson[20,21]
6	$-\frac{\varphi T S_v}{C}$	Peralta and Skaar[23]
7	$-\frac{\varphi\left(T\frac{d\mu_w}{dT}+E_b+E_s+RT\ln(\varphi)\right)}{C}$	Siau[37]
8	$-\frac{\varphi\left(T\frac{d\mu_b}{dT}+E_b+RT\ln(\varphi)\right)}{C}$	Siau and Avramidis[24]
9	$-\frac{\varphi E_b}{C}$	Siau and Avramidis,[24] Peralta and Skaar[23]

$C = RT^2\left(\frac{\partial\varphi}{\partial m}\right)_T$

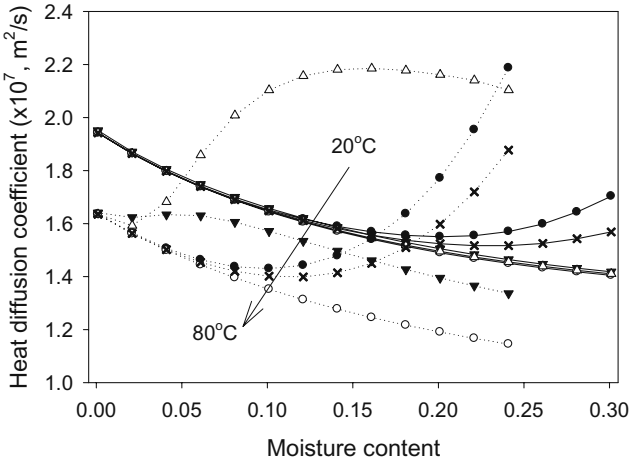

Fig. 10. Heat diffusion coefficient of wood with oven-dried specific gravity of 0.4 at 20°C and 80°C. *Filled circles*, Avramidis model; *open circles*, Perre model; *filled triangles*, Stanish model; *open triangles*, Pang model; *crosses*, Eq. 25

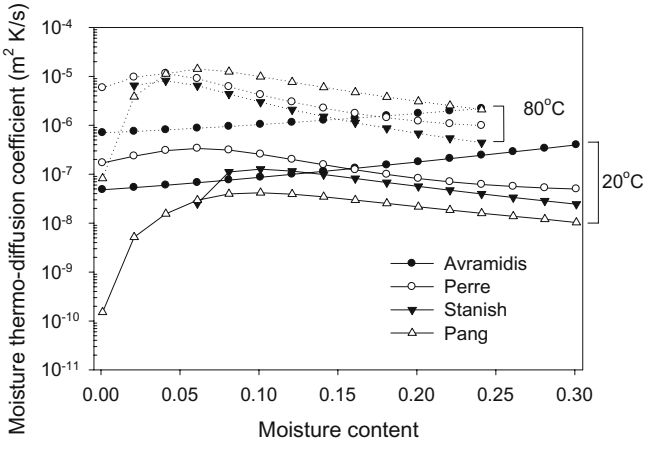

Fig. 11. Moisture thermodiffusion coefficient of wood with oven-dried specific gravity of 0.4 at 20°C and 80°C

increasing K_{22} at higher moisture contents. If K_{22} from Eq. 25 were adopted, the heat diffusion coefficient would exhibit a lower value than in the Avramidis model

$$K_{22} = \frac{1}{\overline{\rho C_p}}\left(\lambda_{eff} + \frac{E_b\overline{\rho C_p}}{0.018C_p}\frac{E_b}{T}\left(\frac{K_{11}\varphi}{RT}\right)\left(\frac{\partial m}{\partial\varphi}\right)\right) \quad (25)$$

The Dufour effect, or moisture thermodiffusion, which causes the heat flux resulting from moisture diffusion, is shown in Fig. 11. However, there is little experimental evidence of the Dufour effect because it cannot be easily measured as the heat diffuses so much more rapidly through wood than does moisture. Therefore, it was difficult to determine what model was more appropriate for explaining moisture thermodiffusion. In addition, the effect of moisture thermodiffusion on the heat transfer rate may not be significant because the heat diffusion is much faster than the moisture diffusion.

The moisture thermodiffusion coefficient (K_{21}) from the Avramidis model increased with increasing moisture content, which is due to a function of the activation energy of bound water. For the other three models, it decreased with increasing moisture content because the enthalpy of bound water (h_b) increases with moisture content.

Conclusions

The driving potential for bound water may differ among researchers, and can be expressed in terms of a number of different state variables. Under isothermal conditions, it does not matter which potential is used in the diffusion equation as long as the appropriate diffusion coefficient is used.

Except for the Avramidis model, the other three models (Stanish, Perre, and Pang) were developed mainly for modeling high-temperature drying above the FSP. The transformation of the four models with different state variables to the same forms results in different phenomenological transport coefficients by moisture content and temperature. There is a certain degree of confusion about the material parameters. This confusion arises from the use of different mathematical expressions and the driving forces assumed. In the case of the isothermal mass transfer coefficient, the moisture diffusion coefficient in the transverse direction by the Stanish and Pang models increased with deceasing moisture content. This contradicts the Avramidis and Perre models as well as numerous experimental results.

The effect of thermal diffusion on the drying process may not be predominant because the nonisothermal state is relatively short. Therefore, Perre's model, which does not consider the thermal diffusion effect, has been used successfully in the drying simulation. However, it may be erroneous in certain cases when the nonisothermal state prevails over the system, such as building physics. The thermodiffusion coefficient, such as from Model 9, may be involved in Perre's model.

Model 9 is more suitable than Model 4 for the Avramidis model. The water vapor movement through the pit should be involved in case of wood with high permeability and high specific gravity, particularly at low moisture content and high temperature, when calculating the moisture diffusion coefficient (Fig. 6b).

Therefore, the application of a model to various wood species would be questionable under a wide range of external conditions, although all four models were verified by experimental results, and satisfactory agreements were obtained for a given material and set of environmental conditions. When developing and adopting new models, examination of whether the transport coefficients have physical meaning and are appropriate over the range of moisture content and temperature under consideration is required.

Acknowledgement This work was supported by the Korea Research Foundation Grants funded by the Korean Government (MOEHRD) (The Regional Research Universities Program/Biohousing Research Institute and KRF-2007-314-F00021).

References

1. Hameury S (2005) Moisture buffering capacity of heavy timber structures directly exposed to an indoor climate: a numerical study. Build Environ 40:1400–1412
2. Siau JF (1984) Transport processes in wood. Springer, Berlin Heidelberg New York, p 245
3. Avramidis S, Englezos P, Papathanasiou T (1992) Dynamic nonisothermal transport in hygroscopic porous media: moisture diffusion in wood. AIChE J 38:1279–1287
4. Stamm AJ (1960) Combined bound-water and water vapor diffusion into Sitka spruce. Forest Prod J 10:644–648
5. Choong ET (1963) Movement of moisture through a softwood in the hygroscopic range. Forest Prod J 13:489–498
6. Siau JF (1995) Wood: influence of moisture on physical properties. Virginia Polytechnic Institute and State University, Blacksburg, p 227
7. Perre P, Moser M, Martin M (1993) Advances in transport phenomena during convective drying with superheated steam and moist air. Int J Heat Mass Transfer 36:2725–2746
8. Whitaker S (1977) Simultaneous heat, mass, and momentum transfer in porous media: a theory of drying. Adv Heat Transfer 13:119–203
9. Stanish MA (1986) The roles of bound water chemical potential and gas phase diffusion in moisture transport through wood. Wood Sci Technol 19:53–70
10. Pang S (1997) Relationship between a diffusion model and a transport model for softwood drying. Wood Fiber Sci 29:58–67
11. Kamke FA, Vanek M (1994) Comparison of wood drying models. Proceedings of 4th IUFRO International Wood Drying Conference, Rotorua, New Zealand, pp 1–21
12. Yeo H, Smith WB (2005) Development of a convective mass transfer coefficient conversion method. Wood Fiber Sci 37:3–13
13. Stanish MA, Schajer GS, Kayihan F (1986) A mathematical model of drying for hygroscopic porous media. AIChE J 32:1301–1311
14. Bories S (1988) Recent advances in modelisation of coupled heat and mass transfer in capillary-porous bodies. Proceedings of 6th International Drying Symposium, pp 46–62
15. Akanni KA, Evans JW (1987) Effective transport coefficients in heterogeneous media. Chem Eng Sci 42:1945–1954
16. Forest Products Laboratory (1999) Wood handbook: Wood as and engineering materials. USDA Forest Service, Forest Products Lab., Madison
17. Simpson WT (1971) Equilibrium moisture content prediction of wood. Forest Prod J 21:48–49
18. Stamm AJ (1959) Bound-water diffusion into wood in the fiber direction. Forest Prod J 9:27–32
19. Perre P, Turner IW (2001) Determination of the material property variations across the growth ring of softwood for use in a heterogeneous drying model. Part 2. Use of homogenization to predict bound liquid diffusivity and thermal conductivity. Holzforschung 55:417–425
20. Nelson RM (1986) Diffusion of bound water in wood. Part 2: a model for isothermal diffusion. Wood Sci Technol 20:235–251
21. Nelson RM (1986) Diffusion of bound water in wood. Part 3: a model for nonisothermal diffusion. Wood Sci Technol 20:309–328
22. Danvind J, Ekevad M (2006) Local water vapor diffusion coefficient when drying Norway spruce sapwood. J Wood Sci 52:195–201
23. Peralta PN, Skaar C (1993) Experiments on steady state nonisothermal moisture movement in wood. Wood Fiber Sci 25:124–135
24. Siau JF, Avramidis S (1993) Application of a thermodynamic model to experiments on nonisothermal diffusion of moisture in wood. Wood Sci Technol 27:131–136
25. Avramidis S, Hatzikiriakos SG (1995) Convective heat and mass transfer in nonisothermal moisture desorption. Holzforschung 49:163–167
26. Hukka A (1999) The effective diffusion coefficient and mass transfer coefficient of Nordic softwoods as calculated from direct drying experiments. Holzforschung 53:534–540
27. Rosenklide A, Arfvidsson J (1997) Measurement and evaluation of moisture transport coefficients during drying of wood. Holzforschung 51:372–380
28. Simpson WT, Liu JY (1991) Dependence of the water vapor diffusion coefficient of aspen (*Populus* spec.) on moisture content. Wood Sci Technol 26:9–21
29. Simpson WT (1993) Determination and use of moisture diffusion coefficient to characterize drying of northern red oak (*Quercus rubra*). Wood Sci Technol 27:409–420

30. Rosen HN (1976) Exponential dependency of the moisture diffusion coefficient on moisture content. Wood Sci 8:174–179
31. Skaar C (1958) Moisture movement in beech below the fiber saturation point. Forest Prod J 8:352–357
32. Comstock GL (1963) Moisture diffusion coefficients in wood as calculated from adsorption, desorption, and steady state data. Forest Prod J 13:97–103
33. Bramhall G (1979) Sorption diffusion in wood. Wood Sci 12:3–13
34. Skaar C, Siau JF (1981) Thermal diffusion of bound water in wood. Wood Sci Technol 15:105–112
35. Siau JF (1983) Chemical potential as a driving force for nonisothermal moisture movement in wood. Wood Sci Technol 17:101–105
36. Siau JF, Zin Z (1985) Nonisothermal moisture diffusion experiments analyzed by four alternative equations. Wood Sci Technol 19:151–157
37. Siau JF (1992) Nonisothermal diffusion model based on irreversible thermodynamics. Wood Sci Technol 26:325–328